Au 10 (SG) 10 : A Chiral Gold Catenane Nanocluster with Zero Confined Electrons. Optical Properties and First-Principles Theoretical Analysis

Franck Bertorelle, Isabelle Russier-Antoine, Nathalie Calin, Clothilde Comby-Zerbino, Amina Bensalah-Ledoux, Stéphan Guy, Philippe Dugourd, Pierre-Francois Brevet, Željka Sanader, Marjan Krstić, et al.

$Au_{10}(SG)_{10}$: A Chiral Gold Catenane Nanocluster with Zero Confined Electrons – Optical Properties and First-Principles Theoretical Analysis

Franck Bertorelle,[†] Isabelle Russier-Antoine, [†]Nathalie Calin,[‡] Clothilde Comby-Zerbino,[†] Amina Bensalah-Ledoux,[†] Stephan Guy,[†] Philippe Dugourd, [†] Pierre-François Brevet, [†] Željka Sanader,[⊥¶] Marjan Krstić, [⊥] Vlasta Bonačić-Koutecký[⊥§] and Rodolphe Antoine[†]**

[†]Univ Lyon, Université Claude Bernard Lyon 1, CNRS, Institut Lumière Matière, UMR 5306 F-69622, LYON, France

‡ Univ Lyon, Ecole Normale Supérieure de Lyon, CNRS Université Lyon 1, Laboratoire de Chimie UMR 5182, 46 allée d'Italie, Lyon, France

[⊥]Center of excellence for Science and Technology-Integration of Mediterranean region (STIM) at Interdisciplinary Center for Advanced Sciences and Technology (ICAST), University of Split, Meštrovićevo šetalište 45, HR-2100 Split, Republic of Croatia

[§] Department of Chemistry, Humboldt Universität zu Berlin, Brook-TaylorStrasse 2, 12489 Berlin, Germany

[¶] Faculty of Science, University of Split, Ruđera Boškovića 33, HR-2100 Split, Republic of Croatia

AUTHOR INFORMATION

Corresponding Author

Rodolphe Antoine : rodolphe.antoine@univ-lyon1.fr.

ABSTRACT. We report a facile synthesis of the $Au_{10}(SG)_{10}$ nanoclusters, where SG stands for glutathione, found to be promising as a new class of radiosensitizers for cancer radiotherapy.The homoleptic catenane structure with two Au_5SG_5 interconnected rings cluster, among different isomer structures, gives the best agreement between theoretical and experimental optical spectra and XRD patterns. This catenane structure exhibits a centrosymmetry-broken structure, resulting in enhanced second harmonic response and new characteristic circular dichroism (CD) signals in the spectral region of 250–400 nm. This is the first determination of the nonlinear optical properties of a ligated cluster with an equal Au-to-ligand ratio, thus without metallic core and therefore zero confined electrons. Insight into the nonlinear and chiro-optical efficiencies arising from interplay between structural and electronic properties is provided by TDDFT approach.

TOC GRAPHICS

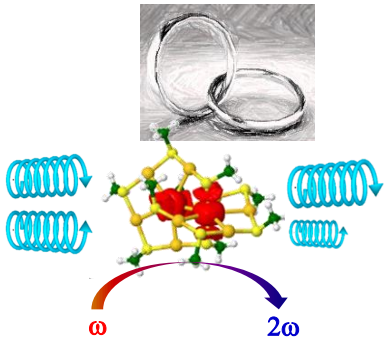

The quest for nanoscale structures with practical bio-applications is rapidly passing from the realm of dreams to reality. Noble metal nanomaterials, in particular gold nanomaterials have received enormous interest in biomedical applications.[1, 2] Ultrasmall gold nanoclusters (NCs)[3, 4] protected by biomolecules such as peptides or proteins[5] may find new opportunities and answer some critical biological considerations.[6] For instance, biocompatibility and renal clearance are two key issues to consider in the design of Au/Ag NCs for biomedical applications.[7] The Xie group recently demonstrated the promising use of ultra-small Au_{10-12}NCs with a naturally occurring peptide (e.g., glutathione or GSH) as the protecting shell as a new class of radiosensitizers for cancer radiotherapy that do not damage normal tissues.[8] These ultra-small NCs were found to be efficiently cleared by kidneys.[8]

In addition to promising radiotherapy properties, noble metal NCs may display NIR emission,[9, 10]and in particular can allow for imaging within the tissue transparency window which, along with their multiphoton excitation properties, may permit deep tissue penetration while minimizing background fluorescence and scattering problems. While recent efforts have been done on the nonlinear optical (NLO) properties determination of small gold and silver NCs,[11-19] the NLO activity of ultra-small gold or silver NCs (with a number of metal atoms lower than 10-12) has not yet been investigated. Note that the 1:1 [Au]:[GS] NCs chemical stoichiometry suggests that Au_{10-12} NCs have a structure similar to the Au(I)-thiolate complexes. Tsukuda and coworkers have shown by ^{197}Au Mössbauer spectroscopy that in $Au_{10}(SG)_{10}$, all gold atoms are bonded to GS ligands, indicating the presence of –Au–S(G)– cyclic structures.[20]Interestingly, it was also shown that the Au-S bonds in the cyclic structures are covalent in nature but with novel elements of electron delocalization.[21] A catenane structure was recently proposed for $Au_{10}(SG)_{10}$based on DFT theoretical investigations.[22] Mechanically interlocked molecules such as catenanes present

remarkable structural and chiroptical properties.[23, 24]The chirality of catenanes can originate either from the presence of chiral elements or from directionality in both rings.[25]Also catenane structures were found to present large optical nonlinearites.[26-28] The asymmetry in the ground and excited states topology plays an essential role in the observed nonlinear optical properties. A high charge transfer character may be observed for catenanes, where charge transfers from one part of the molecule (macrocycle, thread) to the other causes large asymmetries in the molecule and large changes of the dipolar moment in the ground and the excited states. However, here in such interlocked –AuSG- cyclic structures, no metal core (with a delocalized electrons reservoir) is present and the NLO activity for such NCs is expected to be different from the concept of the ligand-core NLO-phore reported for gold and silver NCs.[11-13, 29]

In this letter, we report a facile "one-pot-one-size" synthesis of $Au_{10}(SG)_{10}$NCs characterized by electrospray mass spectrometry. X-ray powder diffraction patterns of $Au_{10}(SG)_{10}$ are collected and compared to simulated X-ray diffraction patterns of different structural species, namely the different catenanes and crown structure. The distinct X-ray diffraction pattern of $Au_{10}(SG)_{10}$ can be utilized as a signature for homoleptic gold-glutathione catenanes. Chiroptical and nonlinear optical properties, i.e. two-photon emission spectra and first hyperpolarizabilities of $Au_{10}(SG)_{10}$are reported. A complementary first-principles theoretical analysis aims at correlating their optical properties with catenane structure NCs with zero confined electrons.

$Au_{10}(SG)_{10}$was prepared as follows: 235 mg of GSH is dissolved in 35 ml of methanol and 2 ml of triethylamine. 100 mg of $HAuCl_4$, $3H_2O$ in 15 ml of water is added and the solution is stirred overnight at ambient temperature. To complete precipitation, 2 ml of 1 M NaOH solution is added and the solution is centrifuged (5 min at 9000 rpm). The unwanted products are removed with cycles of dissolution/precipitation/centrifugation. The resulting powder is dissolved in a minimum

amount of aqueous NH_4OH and then precipitated in methanol. After centrifugation, the powder is dissolved again in 10 ml of water. Then, 2 ml of glacial acetic acid is added and the solution is left undisturbed for 1 hour. Pure $Au_{10}(SG)_{10}$NCs precipitate and are collected by centrifugation. A last cycle of dissolution/precipitation/centrifugation with aqueous NH_4OH–methanol is done before drying the powder. The formation of atomically precise $Au_{10}(SG)_{10}$NCs as the product was confirmed by electrospray ionization (ESI) mass spectrometry (see Figure 1).

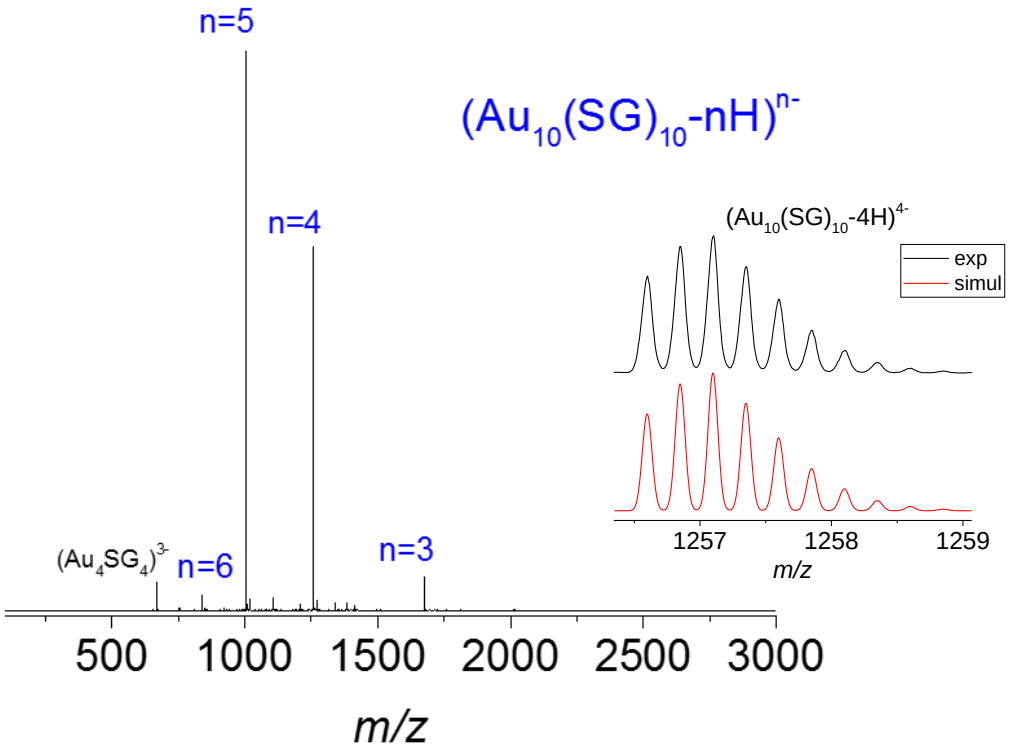

Figure 1: ESI mass spectrum of the as-synthesized $Au_{10}(SG)_{10}$NCs and experimental and simulated isotope distribution of the 4- charge state of Au10(SG)10.The small signals between the n = 5 and n = 4 peaks, as well as between the n = 4 and n = 3 peaks are due to residual $Au_{11}(SG)_{11}$ and $Au_{12}(SG)_{12}$ clusters.

Polyacrylamide gel electrophoresis (PAGE, details in the methods section) of the cluster showed principally one band (under UV illumination, see Fig. S1) confirming the formation of a single

cluster. The sharp band further supports the purity of the sample. We also performed 1D NMR spectroscopy of $Au_{10}(SG)_{10}$. The spectrum of $Au_{10}(SG)_{10}$ presented in Fig. S2 in supporting information has much in common with the ones reported for $Au_{25}(SG)_{18}$[30] and $Au_{18}(SG)_{14}$.[31] On the basis of the chemical shifts of pure GSH and NMR spectra reported for $Au_{25}(SG)_{18}$[30] and $Au_{18}(SG)_{14}$,[31] one can tentatively assign the signals of protons H-2, H-3, H-4, and H-9 of glutathionate in $Au_{10}(SG)_{10}$ since their chemical shifts are not significantly shifted (see Figure S2 in supporting information). Protons H-6 and H-7 (i.e., the β-CH and α-CH2 relative to the thiol group), however, become quite complicated and cannot be simply assigned based solely upon the 1D spectral information.

In an effort to better structurally characterize $Au_{10}(SG)_{10}$NCs, we performed X-ray powder diffraction(XRD). The corresponding experimental XRD intensity profile is shown in Figure 2. In parallel, the DFT method has been used determine structures of the $Au_{10}(SG)_{10}$ NCs based on the results obtained by generic algorithm search method.[22] Influence of different ligands on the structure and stability of the Au_nL_n NCs as a function of their size has been also theoretically investigated previously.[22] In the case of the $Au_{10}L_{10}$NCs with L=SCH_3, a catenane structure containing two interpenetrating pentagons has been found to be the most stable structure. In contrast, the structures containing eight and twelve membered rings interpenetrating each other and crown-like structures lie higher in energy. The structure of the three isomers is shown in Fig. 2. The theoretical powder XRD curves are calculated for the three isomers using the Debye formula[32] (see computational section, for details) and are displayed in Fig. 2.The best agreement is obtained for the lowest homoleptic catenane structure. The theoretical XRD curves of the second and third structures in energy (structure containing two intercalated rings of different size and crown-like structure) have some common features but the agreement is not as good as for the

lowest energy structure. From this XRD analysis, it therefore appears that $Au_{10}(SG)_{10}$adopts a homoleptic catenane structure with two interconnected Au_5SG_5 rings.

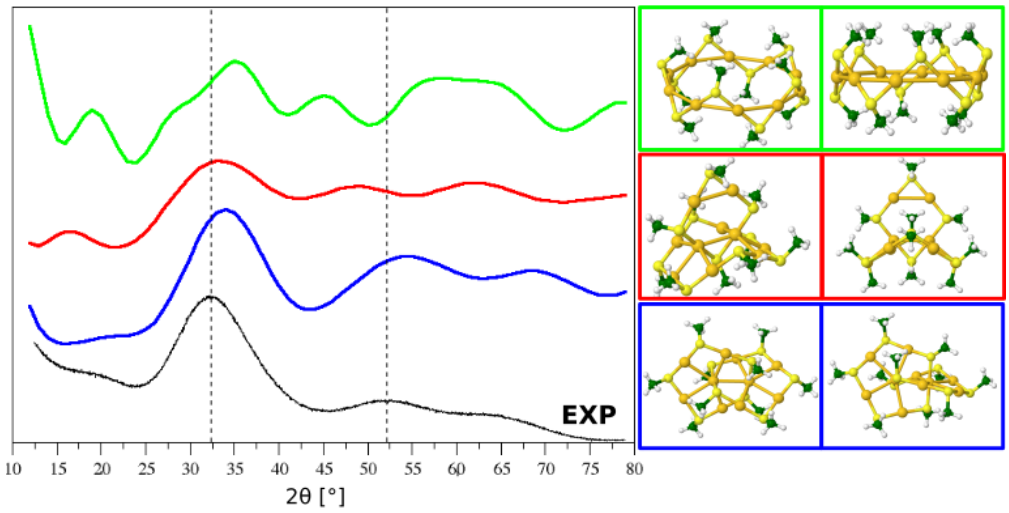

Figure 2: Experimental XRD patterns of $Au_{10}(SG)_{10}$ and simulated patterns for different isomeric structures with two different views (blue : catenane structure, red : structure containing two intercalated rings of different size; green : crown-like structure).

Concerning the optical properties, the linear optical absorption spectrum of the as-synthesized $Au_{10}(SG)_{10}$NCs shows a monotonic increase of absorption below 390 nm and a shoulder at 310 nm (see Figure 3a) with some similarity with the $Au_{10\text{-}12}SG_{10\text{-}12}$ NCs reported by Negishi et al.[33] The one-photon absorption (OPA) spectrum calculated using a TD-DFT approach for the lowest energy catenane structure is shown in Figure S1. The first excited states involved in one-photon absorption (OPA) are located between 400 and 300 nm. They are at the origin of the increasing intensities and are in good agreement with experimental findings. The leading excitations responsible for S_1, S_2 excited states shown also on Figure S1 involve Au-Au aurophilic subunits bound to neighbouring sulphur atoms and arise from the penetration of the two pentagons into each other. Although the metal core is not formed due to the equal ratio of Au atoms and ligands,

aurophilic subunit together with neighbouring sulphur atoms forming two S-Au-S subunits in which the electrons are localized as illustrated by the electron localization function (ELF) in Figure S2, together with additional small amount of delocalized electrons along Au-S bonds of aurophilic Au…Au subunits are responsible for the particular electronic behaviour of the $Au_{10}L_{10}$ NC. The OPA spectrum obtained from the TD-DFT approach for other two higher energy isomers shown in supplementary material (Fig. S3) differ considerably, in particularly for the crown-like structure, from those obtained for the lower energy isomer with a catenane structure. The comparison with the measured features clearly confirms that the catenane structure is responsible for the experimental findings.

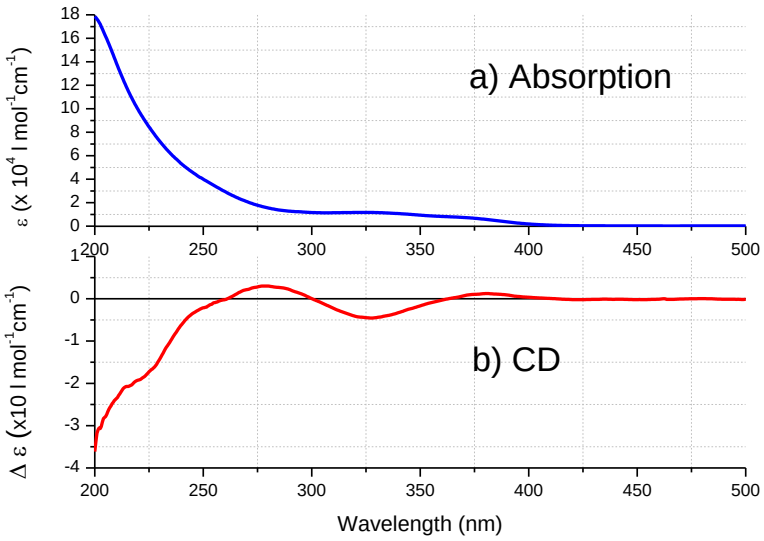

Figure 3: UV-vis absorption (a) and CD spectrum (b) of as-synthesized $Au_{10}(SG)_{10}$ *NCs in aqueous solution.*

Figure 3 shows the optical absorption spectrum for $Au_{10}(SG)_{10}$ in dilute aqueous solution along with its CD spectrum. Chiroptical effects resulting in positive and negative bands in the 250-400 nm region are observed with a strong decrease in Δε below 250 nm (perhaps correlated to the CD

signal of the chiral glutathione ligands[34]). Chirality has been found in L-glutathione-protected gold NCs.[34] The chirality in gold NCs may originate from three possible mechanisms:[35, 36](1) the cluster has an inherently chiral core; (2) the ligands bind in a chiral pattern; (3) the chiral centers in the ligand induce the optical activity in the metal core's electronic structure. In the case of the $Au_{10}L_{10}$NC instead of a metal core, there is an aurophilic Au...Au bond which participates informing two S-Au-S subunits. In order to investigate the origin of chirality in the homoleptic $Au_{10}(SG)_{10}$catenane structure, we performed calculations of the CD spectrum with both an achiral ligand ($-SCH_3$) and a model of a chiral ligand ($-SCH_2CH(CH_3)NH_2$) mimicking the chiral carbon center in the glutathione molecules. Results are shown in Fig. 4. Even with an achiral ligand ($-SCH_3$), the CD spectrum shows chiroptical features resulting in positive and negative bands in the 250-400 nm region. Thus the $Au_{10}(SG)_{10}$NC has an inherently chiral subunit containing two 10-membered rings that are interlocked. This chirality may originate from the mutual interaction of the S-Au-S bonds between the two interconnected rings (as shown in Fig. S1). The calculated CD spectrum with the chiral ligand ($-SCH_2CH(CH_3)NH_2$) is in a slightly better agreement with the experiment(see Fig.4). Note that the used ligand in experiment (e.g. Glutathione peptide) may account for the difference. It is therefore concluded that the origin of the chirality stems from the structure of mutually interacting S-Au-S bonds which are responsible for the leading features of the CD spectrum, with a small contribution from ligand asymmetry.

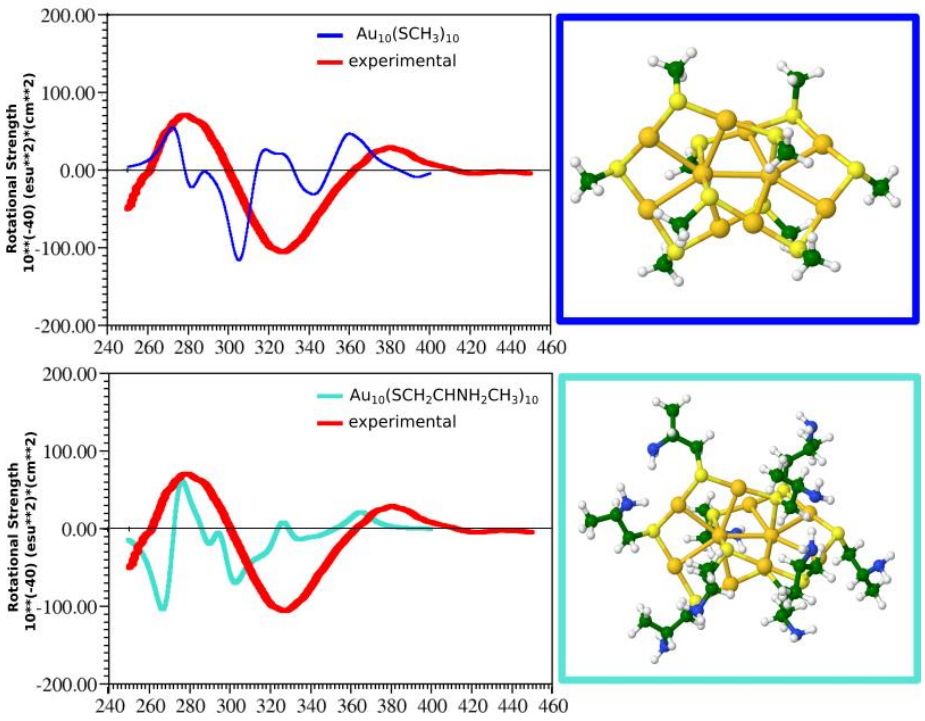

Figure 4: Experimental and simulated (for achiral and chiral L ligand) CD spectra of the Au10L10 NC.

The one and two-photon excited fluorescence (OPEF and TPEF) spectra with an excitation at 420 and 800 nm respectively, were recorded for the $Au_{10}(SG)_{10}$NCs as shown in Figure S4.Upon one-photon excitation at 420 nm of $Au_{10}(SG)_{10}$NCs in aqueous solution, an emission band centered at 510 nm is observed for concentrated (200 µM) solutions (Fig. S4). This spectrum is in qualitative agreement with the photoemission spectrum of $Au_{10}(SPh\text{-}pNH_2)_{10}$reported in the solid state.[37] For TPEF,a broad band in the visible range between 400 and 600 nm centered at about 480 nm was observed. A similar spectrum was obtained for polymeric Au-Cysteine NPs.[38] We attempted to determine the two-photon absorption and emission cross sections for these NCs using the method reported in a previous work.[12] Experimentally, we found that the TPEF cross-section at 800 nm excitation is 0.012 ± 0.005 GM and the TPA cross section 10 ± 4 GM. These experimental cross-sections point to a 2-photon quantum yield 2PQY = σTPE/σTPA for

$Au_{10}(SG)_{10}$NCs of about 1.2×10^{-3}. This quantum yield is the highest 2PQY ever reported for gold-glutathione compounds, however, cross sections are very low as compared to larger gold or silver glutathione protected NCs,[11, 29] and preclude their use as efficient contrast agents for in vitro multiphotonic applications. Due to the fact that the S_1 state in OPA is located at about 400 nm, the lowest two photon transition occurs approximately at 800 nm with a moderate value for its cross-section. The leading excitations within the S_1 state involve Au…Au units together with neighbouring sulphur atoms subunits. The calculations of additional TPA states give rise to S_{15} located at about 600 nm with a higher TPA cross section that is not accessible experimentally (see Fig. S5). However the leading excitations involve also Molecular Orbitals (MO) with large coefficients at gold atoms within the Au…Au subunit. Resonance between OPA and TPA states has not been reached within the manifold of 20 states and the values of transition dipole moments are relatively low.

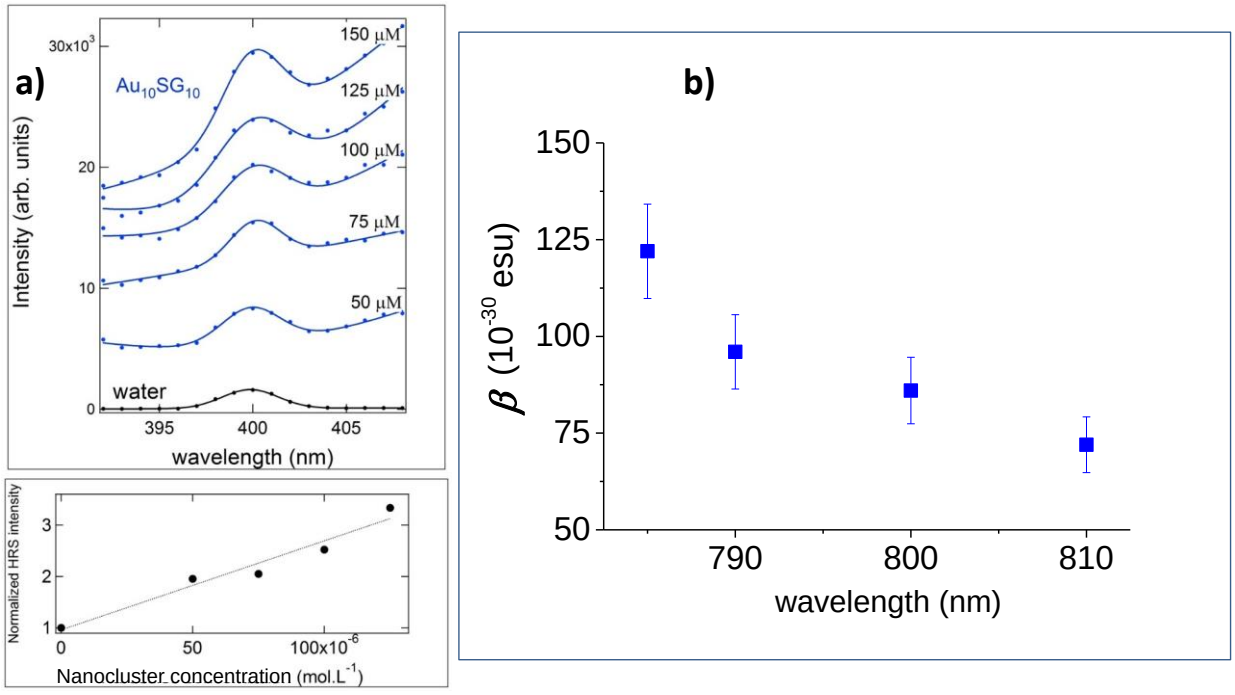

Figure 5: a) HRS line intensity of $Au_{10}(SG)_{10}$ NCs in aqueous solutions for different concentrations (blue circles). Line: fit to a Gaussian function superposed on a linearly increasing function of the wavelength accounting for broadband

multiphoton excited emission. (bottom panel) Plot of the HRS intensity for the $Au_{10}(SG)_{10}$ *NCs in aqueous solution as a function of concentration. The continuous line corresponds to the linear fit. B) Experimental corresponding first hyperpolarizability* β *values as a function of the fundamental wavelength.*

While emission efficiencies are quite low for the $Au_{10}(SG)_{10}$ NCs, one might expect that due to the topology of the catenane structure, a deviation from centrosymmetry should occur leading to large first hyperpolarizabilities. Therefore, the first hyperpolarizability of the as-prepared $Au_{10}(SG)_{10}$NCs was obtained using the hyper-Rayleigh scattering (HRS) technique.[12] The HRS intensity was recorded for several concentrations of the NCs dispersed in aqueous solutions (Figure 5a) and short range spectra were recorded around the HRS wavelength. This experimental procedure is deemed necessary to ensure that the process corresponds to the conversion of two photons at the fundamental frequency into one photon at the harmonic frequency. It is observed in particular that the HRS line is located on top of a strong broadband background. The subtraction of this photoluminescence background was then performed by adjusting the narrow band contribution with a Gaussian function for the HRS line superposed on a linear function of the wavelength accounting for the broadband luminescence background. This subtraction procedure is allowed since the two processes, photoluminescence and HRS, are incoherent. The first hyperpolarizability β determined for an excitation wavelength of 800 nm for the $Au_{10}(SG)_{10}$NCs is found to be $85(9)\times10^{-30}$ esu, only slightly lower than the value reported for Au_{25} clusters, i.e. 128×10^{-30} esu.[12] The calculated first hyperpolarizability β for the lower energy isomers with a catenane structure, see Table S1, is in good agreement with the experimental values. In contrast, calculated β hyperpolarizabilities obtained from the TD-DFT approach for other two higher energy isomers given in supplementary material (Table S1) differ considerably from those obtained for the lower energy isomer with the catenane structure. The crown-like structure is centrosymmetric for SCH_3 ligand and therefore gives rise a zero value for the first hyperpolarizability. In the case

of chiral ligand ($L=SCH_2CH(NH_2)CH_3$) centrosymetric feature is removed and therefore hyperpolarizability have very low values but different from zero (see Table S1). The comparison with the measured values clearly confirms that the catenane structure is responsible for the experimental findings. Interestingly, strong wavelength dependence is predicted for calculated the first hyperpolarizability β values. We managed to record the first hyperpolarizability β between 785 – 810 nm and indeed, an increase in the experimental first hyperpolarizability β values is observed by decreasing the wavelength, consistent with the predicted resonance effect. Note that the experimental position of the S_1 state, estimated at 375 nm, instead of 390 nm for the calculated position may account for the difference observed between experimental and calculated first hyperpolarizability values. A value of ~125×10^{-30} esu is obtained at 785 nm, which is one order of magnitude lower than that of the best SHG dyes used as contrast agents,[39] but in the same range of the hyperpolarizability β values reported for gold clusters with chiral ligands as well as silver alloyed gold NCs.[19]

In summary, we report a simple synthesis to produce atomically precise $Au_{10}(SG)_{10}$ NCs and fully characterize them by ESI mass spectrometry. The homoleptic catenane structure with two Au_5SG_5 interconnected rings cluster gives the best agreement between theoretical and experimental optical spectra and XRD patterns among different isomer structures (in particular crown-like structure). This catenane structure results in the generation of new characteristic circular dichroism (CD) signals in the region of 250–400 nm, whereas no CD signal changes were found with glutathione alone. This chirality originates from a subtle balance between the mutual interaction of the S-Au-S bonds between the two interconnected rings and chiral centers in the ligand inducing the optical activity in the metal core's electronicstructure.$Au_{10}(SG)_{10}$presents a large first hyperpolarizability. The complementary theoretical approach allows for the structural assignment of the experimental

findings as well as for an insight into the nonlinear optical properties of clusters with zero confined electron in the metal core. Altogether aurophilic Au...Au subunits with neighbouring sulphur atoms in catenane structures of $Au_{10}L_{10}$NCs play a key role for their nonlinear optical efficiency.

MATERIALS AND METHODS

Materials. All the chemicals were commercially available and were used without purification. HAuCl4•3H2O, trifluoroacetic acid (TFA), methanol (HPLC grade), GSH (γ-Glu-Cys-Gly, MW 307) were purchased from Carl Roth. NaOH and NH_4OH were purchased from Sigma Aldrich. MilliQ water with a resistivity of 18.2 MΩ cm was used for all experiments.

Electrospray ionization mass spectrometry (ESI-MS). Electrospray ionization MS was performed on a commercial quadrupole time-of-flight (micro-qTOF, Bruker-Daltonics, Bremen, Germany, mass resolution 10 000). The samples were prepared to a final concentration approximately of 50μM in methanol. The samples were analyzed in negative ion mode: each data point was the summation of spectra over 5 mins. External calibration was carried out with a set of synthetic peptides. We used our $Au_{25}SG_{18}$ NCs to optimize the mass spectrometer and defined the measurement uncertainties.

Xray powder diffraction (XRD) measurements. XRD experiments were carried out using a PANalytical EMPYREAN diffractometer with a PIXcel 3D detector using Cu-Kα monochromatic radiation and a High resolution Theta-Theta goniometer. XRD patterns were measured between 12 to 80° in 2θ at room temperature (with a step size of 0.026° and a time per step of 600 sec).

UV-visible, fluorescence and circular dichroism measurements. UV-vis spectra in solution were recorded using an AvaSpec-2048 fiber optic spectrometer and an AvaLight-DH-S deuterium-halogen light source. Fluorescence excitation and emission spectra were obtained using a Fluoromax-4 Horiba fluorimeter.CD spectra were recorded using a home-made setup based on a Photo Elastic Modulator and a lock-in amplifier detection device previously described in ref.[40]

Nonlinear optical measurements. The set-up for Hyper-Rayleigh Scattering (HRS) and two-photon fluorescence emission (TPEF) has been described in details in previous works [11-13]. Briefly, the light source for the HRS and TPEF measurements was a mode-locked femtosecond Ti:sapphire laser delivering at the fundamental wavelength of 780 nm and 950 nm pulses with a duration of about 140 femtoseconds at a repetition rate of 80 MHz. After passing through a low-pass filter to remove any unwanted harmonic light generated prior to the cell, the fundamental beam of about 300 mW was focused by a low numerical aperture microscope objective into a 0.5 cm spectrophotometric cell containing the aqueous solutions. The HRS and TPEF light were collected at an angle of 90° from the incident direction by a 2.5 cm focal length lens. The HRS light was separated from the excitation light by a high-pass filter and a monochromator set at the second harmonic wavelength. The HRS light was then detected with a photomultiplier tube working in the single photon counting regime. For the TPEF signal, the wavelength of the spectrometer (iHR320 spectrometer) was scanned between 350 nm and 750 nm but the same detection unit was used.

Computational. The structural, one and two photon (OPA and TPA) absorption properties of $Au_{10}L_{10}$ (with L=SCH_3) were determined using density functional theory (DFT), time-dependent version (TDDFT)[41],[42] and quadratic response approach as implemented in the DALTON

program package [49]. For gold atoms 19-electron relativistic effective core potential (19e-RECP) was employed[43]. For all atoms, triple zeta plus polarization atomic basis sets (TZVP) have been used[44]. Structural and optical properties (OPA, CD, TPA, β) were determined using the hybrid B3LYP functional[45-47]. Two-photon absorption transition matrices from the ground to the excited state using single residue quadratic response procedure was used for the calculation of TPA the cross section (σ)[48] as implemented in the DALTON[49] program. The Debye formula[51] $\boldsymbol{I(s)} = \sum_{i,j}^{N} \frac{\cos\theta}{(1+\alpha\cos^2 2\theta)} e^{-\frac{Bs^2}{2}} f_i f_j \frac{\sin(2\pi s r_{ij})}{2\pi s r_{ij}}$ was employed to calculate X-ray powder diffraction patterns where *s* is diffraction vector length ($\boldsymbol{s = 2\sin\theta/\lambda}$), θ the diffraction angle, while parameters were set: $\lambda = 1.5406$ Å, $\alpha = 1.01$, the dumping parameter $B = 0.005 nm^2$, atomic scattering factors: f_i atomic number and r_{ij} distance between i^{th} and j^{th} atom.

Supporting Information. PAGE band and 1D NMR spectrum for $Au_{10}(SG)_{10}$. TD-DFT OPA spectrum and views of the electron localization function for the lowest energy structure of $Au_{10}(SCH_3)_{10}$ and for the two higher energy structures. One- and Two-photon excited fluorescence spectra of $Au_{10}(SG)_{10}$. Calculated Two-photon absorption spectrum obtained for the catenane structure of $Au_{10}(CH_3)_{10}$. Calculated first hyperpolarizabilities obtained from the TD-DFT approach for three isomers at different wavelengths. xyz coordinates of the optimized compounds. The following files are available free of charge.

Acknowledgement:

VBK, ZS, MK acknowledge the Center for Advanced Computing and Modelling (CNRM) for providing computing resources of the supercomputer Bura at University of Rijeka in Rijeka, Croatia. Supercomputer and other ICT research infrastructure were acquired through the project

„Development of research infrastructure for laboratories of the University of Rijeka Campus“ which is co-funded by the European regional development fund. The authors acknowledge support from the ICMG FR 2607 NMR plateform (Béatrice Gennaro). The authors also thank Xavier Le Guével and Muriel Jourdan for fruitful discussions.

REFERENCES

1. Muthu, M.S., P. Agrawal, and S. Singh, *Theranostic nanomedicine of gold nanoclusters: an emerging platform for cancer diagnosis and therapy.* Nanomedicine, 2016. **11**(4): p. 327-330.
2. Chen, G., et al., *Nanochemistry and Nanomedicine for Nanoparticle-based Diagnostics and Therapy.* Chem. Rev., 2016. **116**(5): p. 2826-2885.
3. Jin, R.C., *Quantum sized, thiolate-protected gold nanoclusters.* Nanoscale, 2010. **2**(3): p. 343-362.
4. Jin, R., et al., *Atomically Precise Colloidal Metal Nanoclusters and Nanoparticles: Fundamentals and Opportunities.* Chem. Rev., 2016. **116**: p. 10346–10413.
5. Goswami, N., K. Zheng, and J. Xie, *Bio-NCs - the marriage of ultrasmall metal nanoclusters with biomolecules.* Nanoscale, 2014. **6**(22): p. 13328-13347.
6. Zhang, W., et al., *One-step facile synthesis of fluorescent gold nanoclusters for rapid bio-imaging of cancer cells and small animals.* RSC Adv., 2015. **5**(78): p. 63821-63826.
7. Song, X.-R., et al., *Functionalization of metal nanoclusters for biomedical applications.* Analyst, 2016. **141**(11): p. 3126-3140.
8. Zhang, X.-D., et al., *Ultrasmall Au10−12(SG)10−12 Nanomolecules for High Tumor Specificity and Cancer Radiotherapy.* Adv. Mater., 2014. **26**(26): p. 4565-4568.
9. Guevel, X.L., et al., *Ligand effect on the size, valence state and red/near infrared photoluminescence of bidentate thiol gold nanoclusters.* Nanoscale, 2014. **6**(14): p. 8091-8099.
10. Aldeek, F., et al., *Growth of Highly Fluorescent Polyethylene Glycol- and Zwitterion-Functionalized Gold Nanoclusters.* ACS Nano, 2013. **7**(3): p. 2509-2521.
11. Russier-Antoine, I., et al., *Tuning Ag29 nanocluster light emission from red to blue with one and two-photon excitation.* Nanoscale, 2016. **8**(5): p. 2892-2898.
12. Russier-Antoine, I., et al., *Non-linear optical properties of gold quantum clusters. The smaller the better.* Nanoscale, 2014. **6**(22): p. 13572-13578.
13. Sanader, Z., et al., *Two-photon absorption of ligand-protected Ag15 nanoclusters. Towards a new class of nonlinear optics nanomaterials.* Phys. Chem. Chem. Phys., 2016. **18**(18): p. 12404-12408.
14. Ramakrishna, G., et al., *Quantum-Sized Gold Clusters as Efficient Two-Photon Absorbers.* J. Am. Chem. Soc., 2008. **130**(15): p. 5032-5033.

15. Polavarapu, L., M. Manna, and Q.-H. Xu, *Biocompatible glutathione capped gold clusters as one- and two-photon excitation fluorescence contrast agents for live cells imaging.* Nanoscale, 2011. **3**(2): p. 429-434.
16. Knoppe, S., H. Hakkinen, and T. Verbiest, *Nonlinear Optical Properties of Thiolate-Protected Gold Clusters: A Theoretical Survey of the First Hyperpolarizabilities.* J. Phys. Chem. C, 2015. 119: 27676-27682.
17. Philip, R., et al., *Evolution of Nonlinear Optical Properties: From Gold Atomic Clusters to Plasmonic Nanocrystals.* Nano Lett., 2012. **12**(9): p. 4661-4667.
18. Knoppe, S., et al., *Second-Order Nonlinear Optical Scattering Properties of Phosphine-Protected Au20 Clusters.* Ind. Eng. Chem. Res., 2016. **55**: 10500-10506.
19. Van Steerteghem, N., et al., *Symmetry breaking in ligand-protected gold clusters probed by nonlinear optics.* Nanoscale, 2016. **8**: 12123-12127.
20. Kojima, N., et al., *Structural evolution of glutathionate-protected gold clusters studied by means of 197 Au Mössbauer spectroscopy.* Hyperfine Interact., 2013. **217**(1): p. 91-98.
21. Gronbeck, H., M. Walter, and H. Hakkinen, *Theoretical Characterization of Cyclic Thiolated Gold Clusters.* J. Am. Chem. Soc., 2006. **128**(31): p. 10268-10275.
22. Liu, Y., Z. Tian, and L. Cheng, *Size evolution and ligand effects on the structures and stability of (AuL)n (L = Cl, SH, SCH3, PH2, P(CH3)2, n = 1-13) clusters.* RSC Adv., 2016. **6**(6): p. 4705-4712.
23. in *Molecular Catenanes, Rotaxanes and Knots*, C.D.-B. J.-P. Sauvage, Editor. 2007, Wiley-VCH Verlag GmbH. p. I-XIV.
24. Gil-Ramírez, G., D.A. Leigh, and A.J. Stephens, *Catenanes: Fifty Years of Molecular Links.* Angew. Chem. Int. Ed. 2015. **54**(21): p. 6110-6150.
25. Wolf, C., *Dynamic Stereochemistry of Chiral Compounds : Principles and Applications*. 2007, Cambridge: RSC publishing.
26. Gase, T., et al., *Linear and Unanticipated Second-Order Nonlinear Optical Properties of Benzylic Amide [2]Catenane Thin Films: Evidence of Partial Rotation of the Interlocked Molecular Rings in the Solid State.* Adv. Mater., 1999. **11**(15): p. 1303-1306.
27. Niziol, J., K. Nowicka, and F. Kajzar, *Linear and Nonlinear Optical Properties of Selected Rotaxanes and Catenanes*, in *Non-Linear Optical Properties of Matter: From Molecules to Condensed Phases*, M.G. Papadopoulos, A.J. Sadlej, and J. Leszczynski, Editors. 2006, Springer Netherlands: Dordrecht. p. 609-643.
28. Arfaoui, I., et al., *Surface Enhanced Second Harmonic Generation from Macrocycle, Catenane, and Rotaxane Thin Films: Experiments and Theory.* J. Phys. Chem. B, 2006. **110**(15): p. 7648-7652.
29. Russier-Antoine, I., et al., *Ligand-core NLO-phores: a combined experimental and theoretical approach to the two-photon absorption and two-photon excited emission properties of small-ligated silver nanoclusters.* Nanoscale, 2017. **9**: p. 1221-1228
30. Wu, Z., et al., *Probing the Structure and Charge State of Glutathione-Capped Au-25(SG)(18) Clusters by NMR and Mass Spectrometry.* J. Am. Chem. Soc., 2009. **131**(18): p. 6535-6542.
31. Ghosh, A., T. Udayabhaskararao, and T. Pradeep, *One-Step Route to Luminescent Au18SG14 in the Condensed Phase and Its Closed Shell Molecular Ions in the Gas Phase.* J. Phys. Chem. Lett., 2012. **3**(15): p. 1997-2002.
32. Xu, W.W., et al., *Medium-sized Au40(SR)24 and Au52(SR)32 nanoclusters with distinct gold-kernel structures and spectroscopic features.* Nanoscale, 2016. **8**(3): p. 1299-1304.

33. Negishi, Y., K. Nobusada, and T. Tsukuda, *Glutathione-protected gold clusters revisited: Bridging the gap between gold(I)-thiolate complexes and thiolate-protected gold nanocrystals.* J. Am. Chem. Soc., 2005. **127**(14): p. 5261-5270.
34. Schaaff, T.G. and R.L. Whetten, *Giant Gold−Glutathione Cluster Compounds: Intense Optical Activity in Metal-Based Transitions.* J. Phys. Chem. B, 2000. **104**(12): p. 2630-2641.
35. Knoppe, S. and T. Bürgi, *Chirality in Thiolate-Protected Gold Clusters.* Acc. Chem. Res., 2014. **47**(4): p. 1318-1326.
36. Qian, H.F., et al., *Quantum Sized Gold Nanoclusters with Atomic Precision.* Acc. Chem. Res., 2012. **45**(9): p. 1470-1479.
37. Lavenn, C., et al., *Synthesis, characterization and optical properties of an amino-functionalized gold thiolate cluster: Au10(SPh-pNH2)10.* J. Colloid. Inter. Science, 2014. **418**: p. 234-239.
38. Russier-Antoine, I., et al., *Chiral supramolecular gold-cysteine nanoparticles: Chiroptical and nonlinear optical properties.* Prog. Nat. Sci., 2016. **26**: p. 455–460.
39. Reeve, J.E., H.L. Anderson, and K. Clays, *Dyes for biological second harmonic generation imaging.* Phys. Chem. Chem. Phys., 2010. **12**(41): p. 13484-13498.
40. Bensalah-Ledoux, A., et al., *Large-Scale Synthesis of Helicene-Like Molecules for the Design of Enantiopure Thin Films with Strong Chiroptical Activity.* Chem. Eur. J., 2016. **22**(10): p. 3333-3346.
41. Bertorelle, F., et al., *Synthesis, characterization and optical properties of low nuclearity liganded silver clusters: Ag31(SG)19 and Ag15(SG)11.* Nanoscale, 2013. **5**(12): p. 5637-5643.
42. Bonacic-Koutecky, V., et al., *Silver cluster-biomolecule hybrids: from basics towards sensors.* Phys. Chem. Chem. Phys., 2012. **14**: p. 9282-9290.
43. Andrae, D., et al., *Energy-adjusted ab initio pseudopotentials for the second and third row transition elements.* Theor. Chim. Acta, 1990. **77**: p. 123.
44. Weigend, F. and R. Ahlrichs, *Balanced basis sets of split valence, triple zeta valence and quadruple zeta valence quality for H to Rn: Design and assessment of accuracy.* Phys. Chem. Chem. Phys., 2005. **7**: p. 3297.
45. Becke, A.D., *Density-Functional Exchange-Energy Approximation with Correct Asymptotic-Behavior.* Phys. Rev. A, 1988. **38**(6): p. 3098-3100.
46. Becke, A.D., *A New Mixing of Hartree-Fock and Local Density-Functional Theories.* J. Chem. Phys., 1993. **98**(2): p. 1372-1377.
47. Lee, C.T., W.T. Yang, and R.G. Parr, *Development of the Colle-Salvetti correlation-energy formula into a functional of the electron density.* Phys Rev. B, 1988. **37**: p. 789.
48. Norman, P. and K. Ruud, *Microscopic Theory of Nonlinear Optics*, in *Non-Linear Optical Properties of Matter: From Molecules to Condensed Phases*, M.G. Papadopoulos, A.J. Sadlej, and J. Leszczynski, Editors. 2006, Springer Netherlands: Dordrecht. p. 1-49.
49. Aidas, K., et al., *The Dalton quantum chemistry program system.* Wiley Interdisciplinary Reviews: Computational Molecular Science, 2014. **4**(3): p. 269-284.
50. *Dalton, a molecular electronic structure program, Release Dalton2016. (2015), see* http://daltonprogram.org. .
51. Guinier, A., *X-ray diffraction in crystals, imperfect crystals, and amorphous bodies*. 1963, San Francisco: W.H. Freeman.